IEEE Photonics Journal
An IEEE Photonics Society Publication

Temperature Insensitive Vector Bending Sensor Based on Asymmetrical Cascading SMF-PCF-SMF Structure

Volume 9, Number 3, June 2017

Guangwei Fu
Yunpu Li
Qifeng Li
Jiandong Yang
Xinghu Fu
Weihong Bi

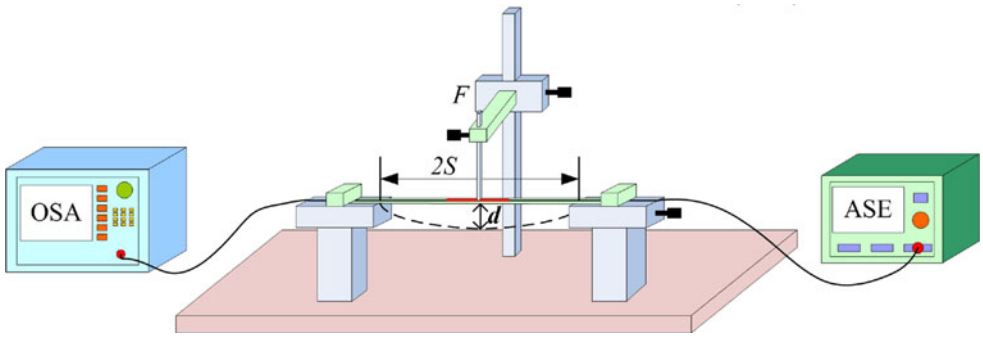

DOI: 10.1109/JPHOT.2017.2692277
1943-0655

Temperature Insensitive Vector Bending Sensor Based on Asymmetrical Cascading SMF-PCF-SMF Structure

Guangwei Fu, Yunpu Li, Qifeng Li, Jiandong Yang, Xinghu Fu, and Weihong Bi

Key Laboratory for Special Fiber and Fiber Sensor of Hebei Province, School of Information Science and Engineering, Yanshan University, Qinhuangdao 066004, China

DOI:10.1109/JPHOT.2017.2692277

Manuscript received January 21, 2017; revised April 2, 2017; accepted April 4, 2017. Date of publication April 7, 2017; date of current version April 25, 2017. This work was supported by the National Natural Science Foundation of China under Grant 61475133, Grant 61575170, and Grant 61675176; in part by the Natural Science Foundation of Hebei province under Grant F2015203270 and Grant F2016203392; in part by the Key Basic Research Program of Hebei province under Grant 16961701D; in part by the Research Fund for Higher Education of Hebei province under Grant QN2016078; and in part by the Qinhuangdao Technology Development Program under Grant 201601B050. Corresponding authors: G. Fu and W. Bi (e-mail: earl@ysu.edu.cn; whbi@ysu.edu.cn).

Abstract: A temperature insensitive vector curvature sensor of photonic crystal fiber (PCF) is presented based on core-offset splicing and waist-enlarged fiber taper. Obvious red and blue shifts in transmission spectrum appear at two symmetrical bending directions with sensor length of 10, 13, 16, and 19 mm and vector curvature of 0.12–1.06 m^{-1}. The longer the sensor length is, the larger the curvature sensitivity is. The corresponding sensitivity with concave bending and convex bending are increased on average by 0.44 and 0.43 nm/m^{-1}, respectively, while the sensor length increases per 1 mm. Moreover, when sensor length is 16 mm, the temperature sensitivity is only 1.73 pm/°C in 20–90 °C; therefore, it has the temperature insensitive property. Obviously, the reported sensor could avert cross-sensitivity of temperature and curvature when measured together. It is prospective being used in industrial production, building monitoring, aerospace, and other fields in view of its easy fabrication, simple structure, and high sensitivity.

Index Terms: Curvature, photonic crystal fiber, core-offset splicing, waist-enlarged taper.

1. Introduction

Fiber optic sensors have the obvious advantages of small size, anti-electromagnetic interference and high sensitivity compared with other sensors [1]–[4]. In recent years, flexural measurement technique gets more and more widely used in the fields of machinery, bridge, architectural structure and other areas such as health monitor at bending deformation of high precision instruments and equipment. The structure parameters such as stress, strain, curvature and so on in the construction engineering especially, which could reflect the characteristics of the materials and structural mechanics, are the foundation of assessing the state of building structure. There are a lot of reports based on different structure optical fiber curvature sensors, such as Michelson interferometer [5], Fiber Bragg Grating (FBG) [6], [7], Photonic Crystal Fiber (PCF) [8], [9], and other types of sensors with microstructures [10], which could be well applied to the curvature measurement.

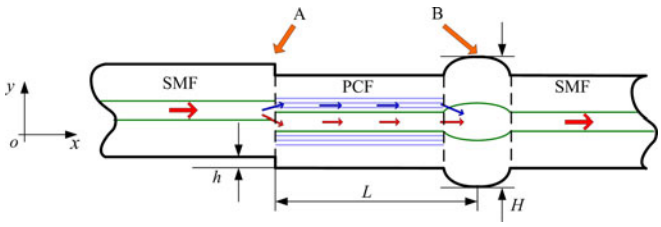

Fig. 1. Structure of the sensor.

Pengcheng Geng [11] *et al*. reported a curvature vector sensor on the base of two long period orthogonal FBGs getting their curvature vector measurement. Dong [12] *et al.* designed an optical fiber bending sensor with core shift structure, its bending sensitivity of 2.826 nm/cm^{-1}. Li *et al.* [13] presented their curvature sensors on the strength of waveguide array optical fiber with the sensitivity of 10 nm/m^{-1} within the curvature scope of 0-10 m^{-1}. However, the sensors mentioned above exist some problems, such as the complex manufacture of FBG sensor, the cross-sensitivity when measuring temperature and curvature together, which seriously influence the measurement precision of the sensor. Due to its simple manufacture, compact structure and the characteristic of PCF as being insensitive to temperature, research about Mach-Zehnder PCF sensor is gaining increasing attention.

In view of the analysis above, a PCF curvature sensor is proposed based on core-offset splicing and waist-enlarged fiber taper in this paper. The curvature sensor is made by technique of core-offset splicing and excessive fusion splicing for PCF, using ordinary commercial splicing machine, thus a PCF curvature sensor with core-offset splicing and waist-enlarged fiber taper is prepared by analyzing the influence of splicing parameters on the sensor spectrum. The relationship of sensing arm length and interference period is presented by means of core-offset splicing with axial asymmetry to realize the curvature vector measurement. Experimental study on the curvature of the sensor and temperature characteristics has been done, and the results show that the sensor has high sensitivity of curvature response and can detect the bending curvature on both directions and can then solve the problem of cross-sensitivity of temperature and curvature when measured together.

2. Basic Principle

The structure of the core-off splicing and waist-enlarged fiber taper is shown in Fig. 1. It is made by core-offset splicing one end of the PCF with the single-mode fiber (SMF) on the direction of *y* axis, and excessively fusion splicing the other end with another SMF. An asymmetrical cascading SMF-PCF-SMF structure is presented.

As shown in Fig. 1, *x* represents the abscissa axis of the sensor cross sections, *y* is its vertical axis, and *L* is the fusion splicing length of PCF, namely the length of the core-offset splicing and waist-enlarged fiber taper. *H* is the diameter of splicing joint, and *h* is the offset of PCF. When the fusion splicing SMF with PCF, different splicing situation would cause different change of fiber structure at fusion splices and then give rise to mismatch of fiber mode field; therefore, the input light at the core-offset splicing joint A and excessive fusion splicing point B would separately produce light splitting and combining phenomenon. When the light passes through the core-offset splicing joint A, a part of the light is coupled into the PCF cladding, and the other part of the light continues to remain in the PCF core, transferring light by fiber cladding mode and core mode, respectively. Due to the effective refractive index difference between the PCF cladding mode and the core mode, the two parts of the light transferring through cladding mode and core mode can lead to the phase difference after certain optical transmission distance. If the cladding mode and the core mode are regarded as the sensing arm and the reference arm of the interferometer respectively, they will intervene at the excessive fusion splicing point B, forming a Mach-Zehnder interferometer.

According to the theory of double beam interference, the intensity of the output light [14] of this Mach-Zehnder interferometer is

$$I = I_1 + I_2 + 2\sqrt{I_1 I_2}\cos\varphi \tag{1}$$

where I_1 and I_2 are the intensity of the transmission light through fiber core mode and cladding mode respectively. φ is the phase difference produced by these two transmission light, namely

$$\varphi = \frac{2\pi\left(n_{\text{eff}}^{r} - n_{\text{eff}}^{d}\right)L}{\lambda} = \frac{2\pi\left(\Delta n_{\text{eff}} L\right)}{\lambda} \tag{2}$$

where n_{eff}^{r} and n_{eff}^{d} are the effective refractive indexes of fiber core mode and cladding mode, respectively. λ is the light transmitting wavelength in the optical fiber, Δn_{eff} is the effective refractive index difference between fiber core mode and cladding mode. The interference spectrum would appear in a series of maximum and minimum values in the transmission process, and the maximum value will appear at the value $\varphi = 2\pi m$, reaching

$$\frac{2\pi\Delta n_{\text{eff}} L}{\lambda} = 2\pi m. \tag{3}$$

In (3), $m = 1, 2, 3\ldots\ldots$; thus, the central wavelength λ_m of the m order interference fringe could be expressed as

$$\lambda_m = \frac{\Delta n_{\text{eff}} L}{m}. \tag{4}$$

When the external environment makes the fiber bending, the effective refractive index of the fiber core mode and cladding mode of PCF will be changed due to the elastic-optic effect of the fiber, and then affects the optical path difference between fiber core mode and cladding mode, causing interference spectrum shifting. Therefore, it can be known that the center wavelength shift [15] of the m order interference fringe of the sensor caused by the change of the external curvature is

$$\Delta\lambda_m = \frac{\left(\Delta n_{\text{eff}} + \Delta n\right)L}{m} - \frac{\Delta n_{\text{eff}} L}{m} = \frac{\Delta n L}{m} \tag{5}$$

where Δn is the variation of the effective refractive index difference between PCF fiber core mode and cladding mode. The cylindrical symmetry of the fiber structure is destroyed on account of core-offset splicing and excessive fusion splicing. Especially, when the light is passed through the core-offset splicing joint A, a part of the fiber core fundamental mode is coupled into the cladding, which leads to the energy of the light in the forward direction along y axis in the transmission process is greater than that in the negative direction of y axis. When the fiber is bent, the increase of the effective refractive index near the outside of the fiber axial is greater than that of the inside. Therefore, when the sensor is concave to the bending, the fiber core mode is close to the outer side of the fiber axis, and the increases of the effective refractive index of the cladding mode will be less than that of the fiber core mode, causing the Δn positive, and then $\Delta\lambda_m$ positive, which indicates that the interference fringe moves toward to the long wave direction. Conversely, when the sensor fiber is convex to the bending, the interference fringes will be shifted to the short wave direction. Therefore, the direction and the magnitude of the bending curvature can be determined by detecting the shift direction and shift distance of the center wavelength of certain order interference fringes. By using (5), it can be evaluated that when Δn is certain, the longer L is, the greater the optical path difference between fiber core mode and cladding mode accumulated on L will be, then the larger the corresponding interference fringes shift of the sensor will be, and the higher the sensitivity of the sensor will be. Therefore, the length of the sensor can be increased to improve the sensitivity of the sensor.

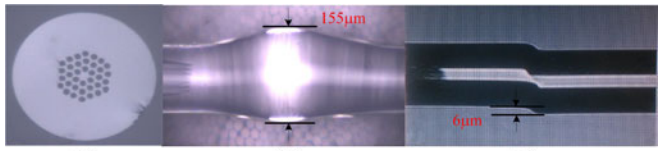

Fig. 2. (a) Cross-section of SM-10 type PCF. (b) Waist-enlarged fiber taper caused by excessive splicing. (c) Fiber with core-offset splicing.

3. Experiment and Results Analysis

3.1 Preparation of the Sensors

The SM-10 type PCF solid core optical fiber used in the experiment is supplied by Yangze Optical Fiber & Cable company. It has three layers of air holes arranged in a hexagonal structure. The cladding diameter is 125 μm, the fiber core diameter is 9.5 μm, and its end face is shown in Fig. 2(a). FITEL-S178A optical fiber splicer is used for sensor preparation. The splice of PCF and SMF is carried out by manual splicing. Firstly, strip the coating of a PCF with stripping pliers, then place it on the splicing machine to splice it with SMF after alcohol wiping. Finally, different splicing joints can be obtained by adjusting different splicing methods. By increasing the impelling quantity of two sides of the optical fiber spliced, the waist-enlarged fiber taper with excessive splicing is produced, as shown in Fig. 2(b). The diameter of splicing joint H is 155 μm. In the splicing process, the axial asymmetry of the fiber is caused by manual misalignment, then a core-offset splicing joint is formed, the offset of h is 6 μm, as shown in Fig. 2(c).

In the experiments, the curvature sensors of core-offset splicing and waist-enlarged fiber taper are prepared with the sensor length of 10 mm, 13 mm, 16 mm, and 19 mm, respectively, and their transmission spectrum are shown in Fig. 3.

In Fig. 3, we can see that with the increase of the length of the sensors, the number of the interference period of the transmission spectrum increases, that is, the interference fringe spacing decreases. It can be derived from (4), the fringe spacing $\Delta\lambda_m$ is

$$\Delta\lambda = \frac{{\lambda_{m'}}^2}{\Delta n_{\text{eff}} L}. \tag{6}$$

Due to the close proximity of m order interference fringes center wavelength and m+1 order's, λ_m and λ_{m+1} can approximately be regarded as equal amounts $\lambda_{m'}$ for convenience.

According to (6), it can be concluded that with the increase of the sensor length L, the fringe spacing $\Delta\lambda_m$ decreases gradually, and the number of interference period increases gradually, which is consistent with the experimental results.

By analyzing a large number of experimental results, it is found that if the fiber misalignment and the diameter of the waist-enlarged fiber taper are too small, it is not easy to stimulate the cladding mode transmission. And the large misalignment and diameter of the waist-enlarged fiber taper can also cause the transmission energy loss too much, which leads to the difficulty of detecting the formed interference fringe.

Therefore, after repeated experiment studying, it is accepted that when the fiber displacement is 6 μm on y direction for SMF and PCF, and the diameter of the waist-enlarged fiber taper is 155 μm, a curvature sensor with core-offset splicing and waist-enlarged fiber taper, possessing distinct interference fringe and obvious shift, will then be produced.

3.2 Spectral Analysis

The transmission spectra with sensor length of 10 mm, 13 mm, 16 mm and 19 mm shown in Fig. 3 are carried out by fast Fourier transform respectively, which can be used to analyze the main modes of the interference in Mach-Zehnder interferometer, as shown in Fig. 4.

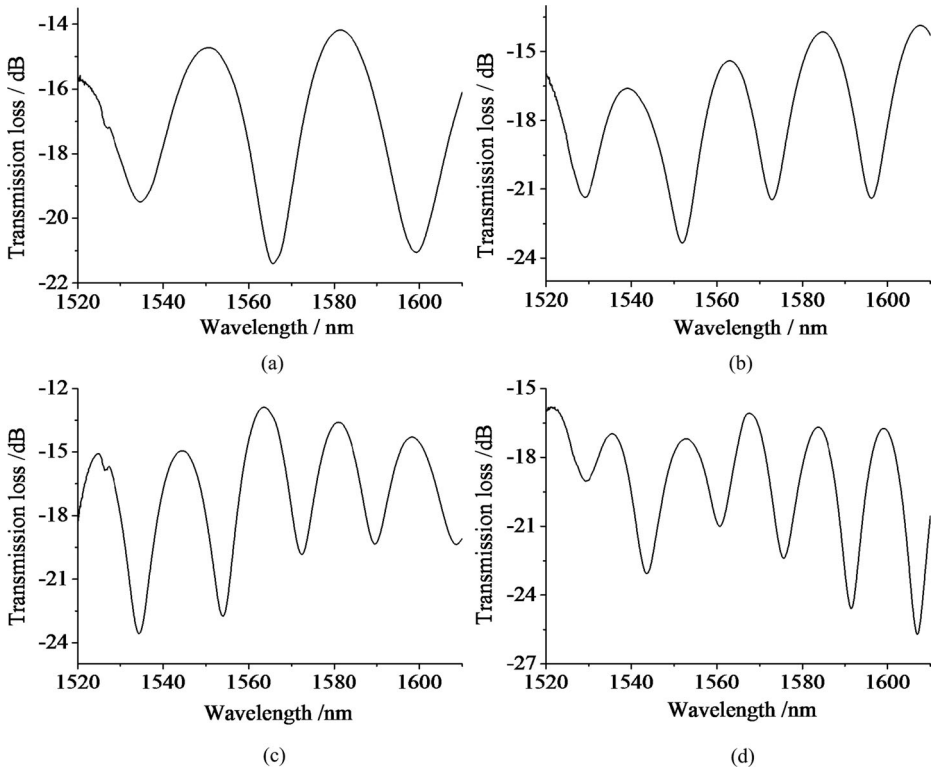

Fig. 3. Transmission spectrum of the curvature sensors with different length. (a) 10 mm. (b) 13 mm. (c) 16 mm. (d) 19 mm.

Fig. 4 shows that each of the fast Fourier spectrum in addition to the core model with spatial frequency of 0.0 nm^{-1}, there is only one main peak, and its amplitude is greater than other small peaks. Therefore, the interference between two modes in Mach-Zehnder interferometer is generated by mutual interference with base model transmitted by the fiber core and the mode corresponding to the main peak. After the calibration is obtained, for sensor length of 10 mm, 13 mm,16 mm and 19 mm, the corresponding main spatial frequency spectrum on Fourier spectrum is 0.033429 nm^{-1}, 0.044486 nm^{-1}, 0.055479 nm^{-1} and 0.066590 nm^{-1}.

The phase difference φ is carried out by Taylor equation, then we get

$$\varphi \approx \varphi_0 + \frac{2\pi\Delta\lambda'}{{\lambda_0}^2}\Delta n_{\text{eff}} L \tag{7}$$

where λ_0 is the central wavelength of the interference fringe, set as 1550 nm. $\Delta\lambda'$ is the difference between wavelength λ of the light transmitted in the fiber and the central wavelength λ_0 of the interference fringe. For the interference spectrum of cosine type, there exists

$$\cos(\Delta\varphi) = \cos\left(2\pi\xi\Delta\lambda'\right). \tag{8}$$

Therefore, the spatial frequency ξ can be deduced by (7) and (8)

$$\xi = \frac{1}{{\lambda_0}^2}\Delta n_{\text{eff}} L. \tag{9}$$

Using the main spatial frequencies obtained from the experiment in Fig. 4, combined with (9), it can be figured out that the effective refractive index difference Δn_{eff} between fiber core and cladding mode are 0.00803, 0.00822, 0.00833, and 0.08420, corresponding to the sensor length of 10 mm, 13 mm, 16 mm, and 19 mm, respectively.

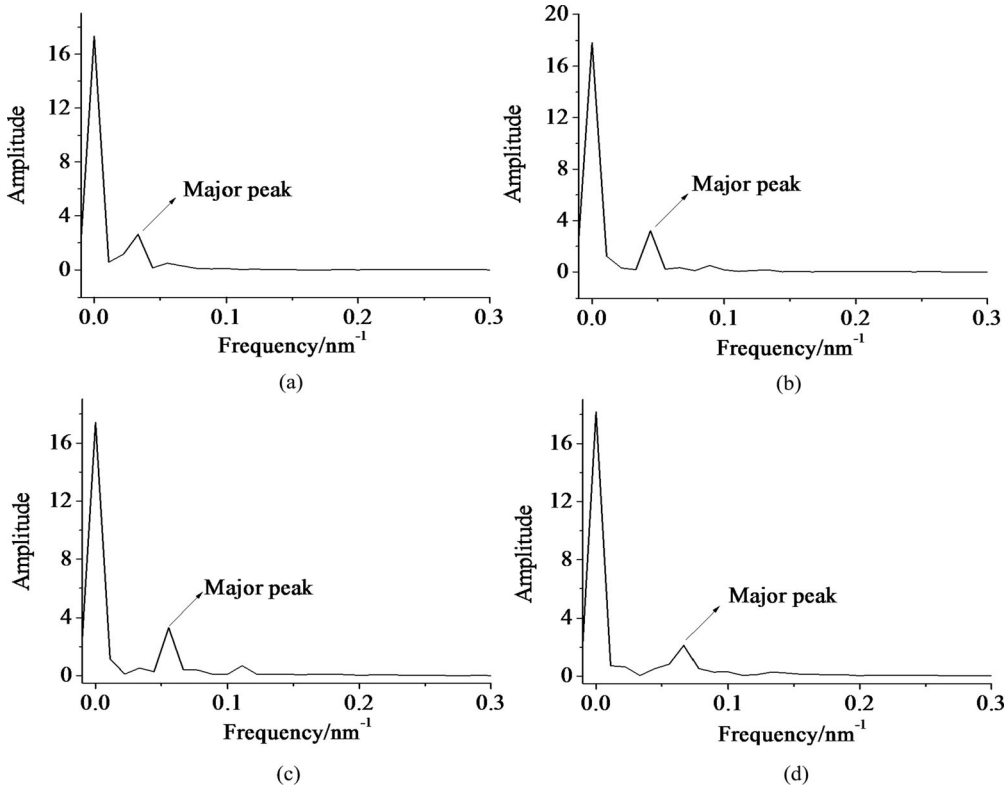

Fig. 4. Fourier spectrum of the transmission spectrum with different sensor length. (a) 10 mm. (b) 13 mm. (c) 16 mm. (d) 19 mm.

TABLE 1
Difference of Effective Refractive Index Between High-Order Mode and the Fundamental Mode

Group	High modes	The effective index difference between high modes and LP_{01}
1	LP_{11}	0.007291
2	LP_{21}	0.015869
3	LP_{02}	0.019145
4	LP_{31}	0.021859
5	LP_{12}	0.027538

The effective refractive index in PCF transmission of several groups with high order mode rate can be obtained by using a full vector finite element method, and the effective refractive index difference between the high-order mode and the fundamental mode are calculated, the results are shown in Table 1.

Comparing the data in Table 1, it can be known that the effective refractive index difference between the fundamental mode and LP_{11} mode is 0.007291. The result is approximately consistent with the effective refractive index difference of the two modes gained from experiment. Therefore, it is believed that the interference spectrum obtained in the experiment is caused by the interference between the fundamental mode and the LP_{11} mode.

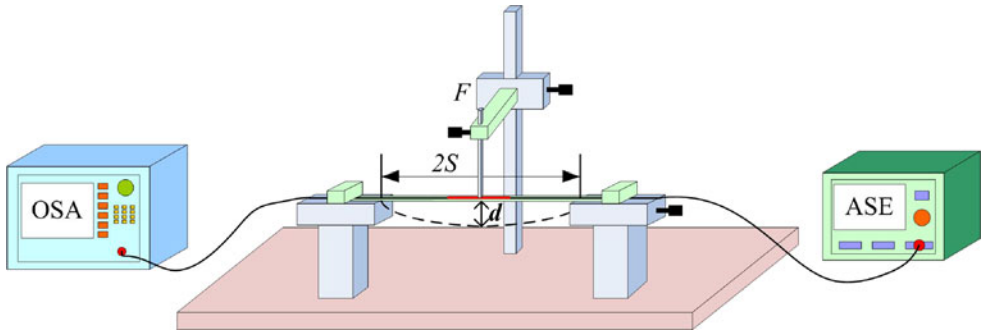

Fig. 5. Curvature measurement experimental system.

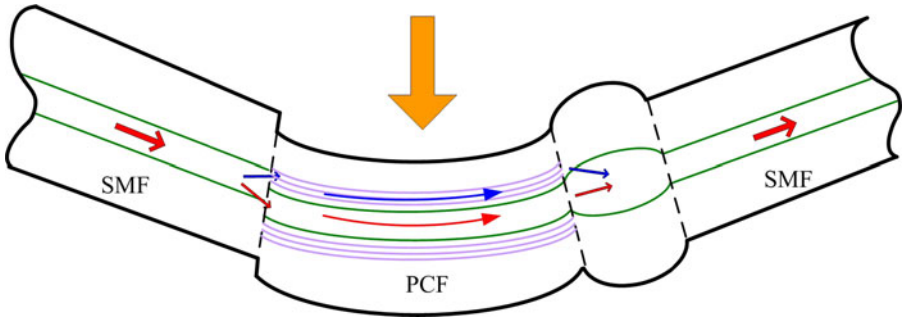

Fig. 6. Schematic diagram of the sensor for concave bending.

3.3 Curvature Sensing Experiment

The schematic diagram of the experimental system for curvature measurement is shown in Fig. 5. In experiments, the wavelength range of Amplified Spontaneous Emission(ASE) broadband light source is within 1520-1610 nm, and the experimental data is recorded by AQ6375 type Optical Spectrum Analyzer (OSA).

In the curvature measurement system, both ends of a steel ruler are level fixed on the two three-dimensional adjustable platform. Move the top of the lifting platform F on the steel ruler up and down, and then can change different distanced on the underdraught of the ruler to achieve different degrees of bending steel ruler. The curvature expression [16] is obtained by the movement distance of the lifting platform and the distance between two three-dimensional adjustable platforms

$$C = \frac{1}{R} = \frac{2d}{d^2 + S^2} \tag{10}$$

where R is the bending radius of curvature, d is the movement distance of the lifting platform, $2S$ is the distance between two three-dimensional adjustable platforms, its initial value is 260 mm.

In order to study the influence of the length of the sensor on its curvature sensitivity, the sensor lengths of 10 mm, 13 mm, 16 mm, and 19 mm were used to carry out the curvature sensing experiment. In the experiment, the sensor is fixed on the lower surface of the steel ruler, the ruler and sensor must fit tightly to ensure the bending degree of change the steel ruler is to change the bending degree of the sensor. SMF at both ends of the sensor are connected with the light source (ASE) and the OSA, respectively. The distance between the two three-dimensional platforms is kept constant during the experiment. By changing the moving distance of the lifting platform to change the curvature, a total of 9 transmission spectra are recorded for each decrease in 1 mm. According to (10), the corresponding curvature variation range is 0.12$\sim$1.06 m^{-1}. The schematic diagram of the sensor for concave bending is shown in Fig. 6.

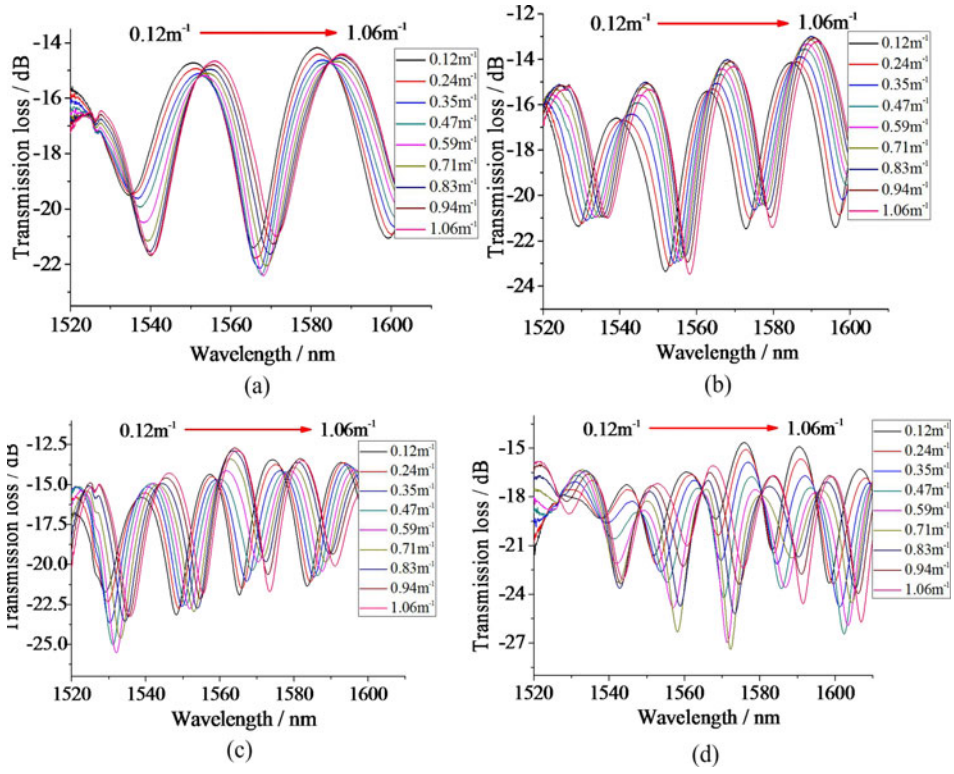

Fig. 7. Transmission spectrum of different curvatures with different sensor length for concave bending. (a) 10 mm. (b) 13 mm. (c) 16 mm. (d) 19 mm.

Different curvature is obtained according different distance at lower pressure. Observing the transmission spectra, the transmission spectrum of different curvature with different sensor length for concave bending is shown in Fig. 7.

As seen from Fig. 7, with the increase of the moving distance of the lifting platform, the curvature of the sensor bending becomes larger and larger. The transmission spectrum is gradually shifting to the long wave direction, which has obvious red shift phenomenon. Calculate the wavelength shift of the transmission spectrum in the vicinity of 1590 nm trough, and the relationship between wavelength shift and curvature can be obtained, as shown in Fig. 8.

It can be seen from Fig. 8, for the sensor with the length of 10 mm, 13 mm, 16 mm and 19 mm for concave bending, the corresponding curvature sensitivity is 5.84 nm/m^{-1}, 7.33 nm/m^{-1}, 8.32 nm/m^{-1}, and 9.87 nm/m^{-1}, respectively, and the linearity R^2 is 0.99361, 0.99047, 0.99662 and 0.99246, respectively, showing a good linear relationship between the wavelength shift and the change of curvature. This is because when the bending curvature of the sensor changes, the elastic-optic effect of the fiber will make the effective refractive index of fiber core mode and cladding mode in the PCF sensing area change accordingly, then n^r_{eff} and n^d_{eff} will be increased. When the fiber is bent, the increase of the model effective refractive index near to the outer side of the fiber axial is greater than that near to the inner side. It can be known from Fig. 6 that the fiber core mode is close to the outer side of the fiber axis when the sensor is concave to bending, as a result, the change of n^r_{eff} is larger than n^d_{eff}. By (5), it is known that the difference between the fiber core mode and the cladding mode is positive, and the value of $\Delta\lambda_m$ is positive, which indicates that the transmission spectrum shifts to the direction of long wave. With the increase of the bending degree, the difference between the fiber core mode and the cladding mode is gradually increasing, and the absolute value of $\Delta\lambda_m$ is also increasing. Consequently, with the increase of curvature, red shift will occur for the transmission spectrum of the sensor, and as the sensor length increases, its curvature sensitivity also increases accordingly. The experimental results are in good agreement with the

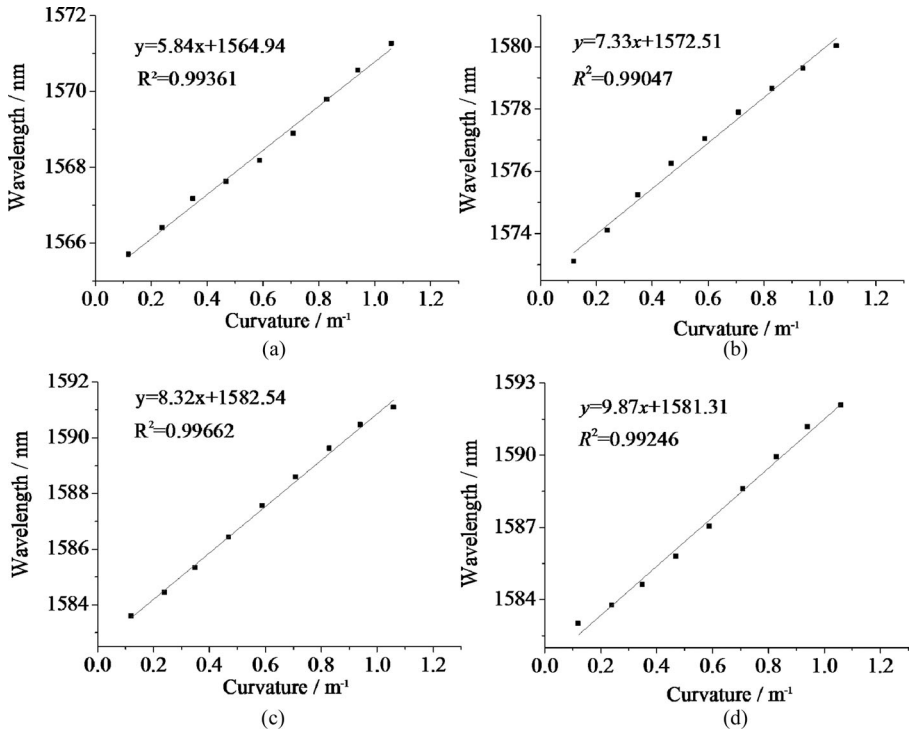

Fig. 8. Relationship between wavelength shift and curvature for concave bending with different sensor length. (a) 10 mm. (b) 13 mm. (c) 16 mm. (d) 19 mm.

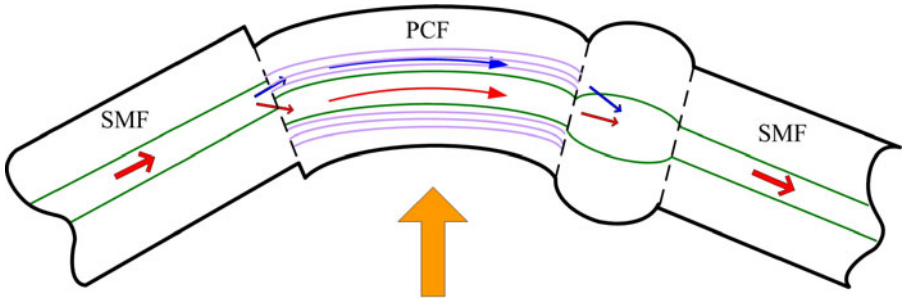

Fig. 9. Schematic diagram of sensor convex bending.

theoretical analysis. Make the sensor turn 180 degrees based on the fiber center axis as the center shaft and then fix it on the lower surface of the steel ruler, then do the same operation by changing the moving distance of the lifting platform to change the curvature. Pressing downward the ruler is equivalent to make the sensor convex bending. Schematic diagram of the sensor convex bending is shown in Fig. 9.

As the fiber curvature increases, an obvious blue shift phenomenon will happen to the transmission spectrum corresponding to different curvature. The transmission spectra corresponding to the different curvature for convex bending are shown in Fig. 10.

It can be viewed from Fig. 10, along with the increasing bending curvature of the sensor, the transmission spectrum shifts to the direction of short wave. Calculating the wavelength shift of the transmission spectrum near to 1590 nm trough, it comes to the relationship between wavelength shift and curvature, as shown in Fig. 11.

Fig. 11 shows that for sensors with the length of 10 mm, 13 mm, 16 mm and 19 mm for convex bending, the corresponding curvature sensitivity is -5.79 nm/m^{-1}, -7.31 nm/m^{-1}, -8.31 nm/m^{-1},

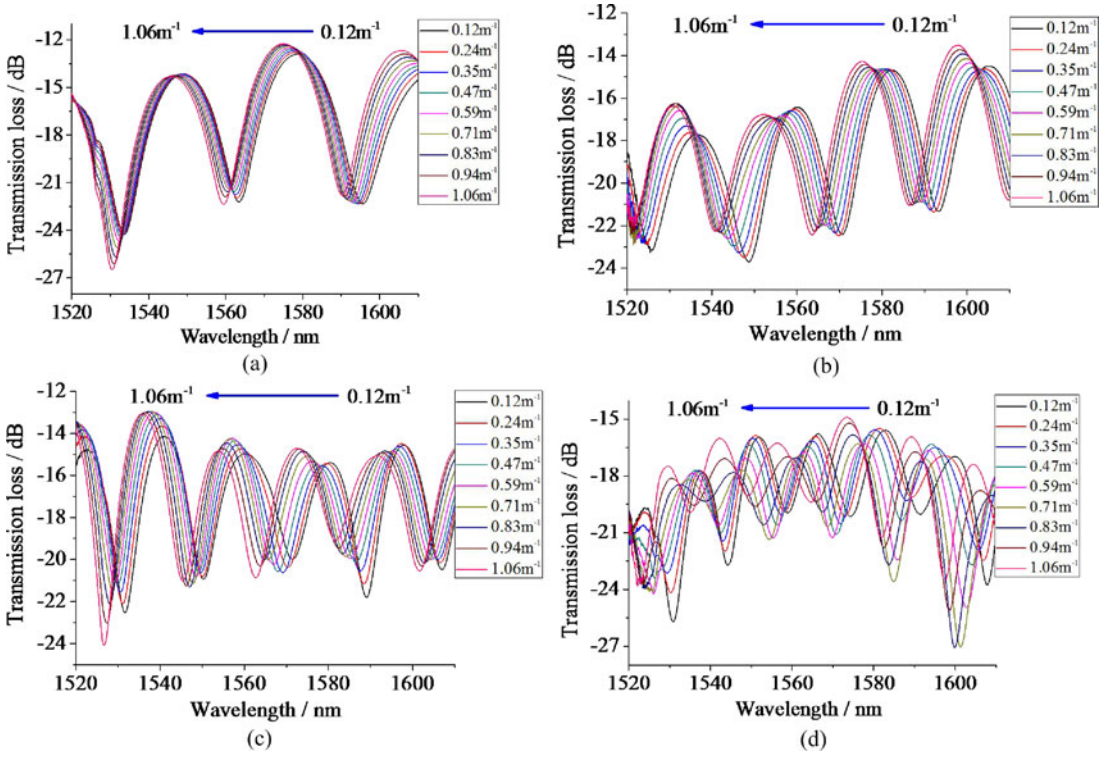

Fig. 10. Transmission spectrum corresponding to different curvatures for convex bending with different sensor length. (a) 10 mm. (b) 13 mm. (c) 16 mm. (d) 19 mm.

and -9.74 nm/m^{-1} respectively. And the linearity R^2 is 0.99869, 0.9945, 0.99395, and 0.99412, respectively, illustrating a good linear relationship between the wavelength shift and the curvature change. The negative sign only indicates the direction of wavelength shifts. It is attributed to the change of the bending curvature of the sensor, the increase of the model effective refractive index near to the outer side of the fiber axial is greater than that near to the inner side. As shown in Fig. 9, when the sensor is convex to bending, the fiber core mode is close to the inner side of the fiber axis, the change of n^r_{eff} is smaller than n^d_{eff} consequently. Thus, the difference between the fiber core mode and the cladding mode is negative. When increase the bending degree, the absolute value of $\Delta\lambda_m$ gradually increase. As a consequence, known from (5), with the increase of curvature, blue shift will happen to the transmission spectrum of the sensor. With the sensor length increases, its curvature sensitivity increases correspondingly. The experimental results are greatly consistent with the theoretical analysis.

From the curvature experimental results, we can know the transmission spectra will shift with curvature changes at 10 mm ~19 mm sensor length. The part of transmission spectra became irregular, which is unfavorable to detection with the length of 19 mm. When the sensor length less than 10 mm, the transmission spectra has a little shift, and also unfavorable to detection. Therefore we design the experiment at 10 mm ~19 mm sensor length. In order to further verify the relationship between the length of the sensor and the sensitivity of curvature, namely with the increase of the length of the sensor, the sensitivity of curvature increases. Curvature experiments have been done on the sensor length of 10 mm, 13 mm, 16 mm, and 19 mm, respectively. The results show that for concave bending red shift has been happened to all the sensors in the curvature range of 0.12~1.06 m^{-1} near the trough of 1590 nm, and the shifts to the long wavelength are 5.56 nm, 6.9 nm, 7.49 nm and 8.31 nm respectively, the corresponding curvature sensitivity are 5.84 nm/m^{-1}, 7.33 nm/m^{-1}, 8.32 nm/m^{-1} and 9.87 nm/m^{-1} separately. Inversely for convex bending it occurs to blue shift at all the sensors, and the shifts to the short wavelength are 5.34 nm, 6.88 nm, 7.35 nm, and 9.47 nm

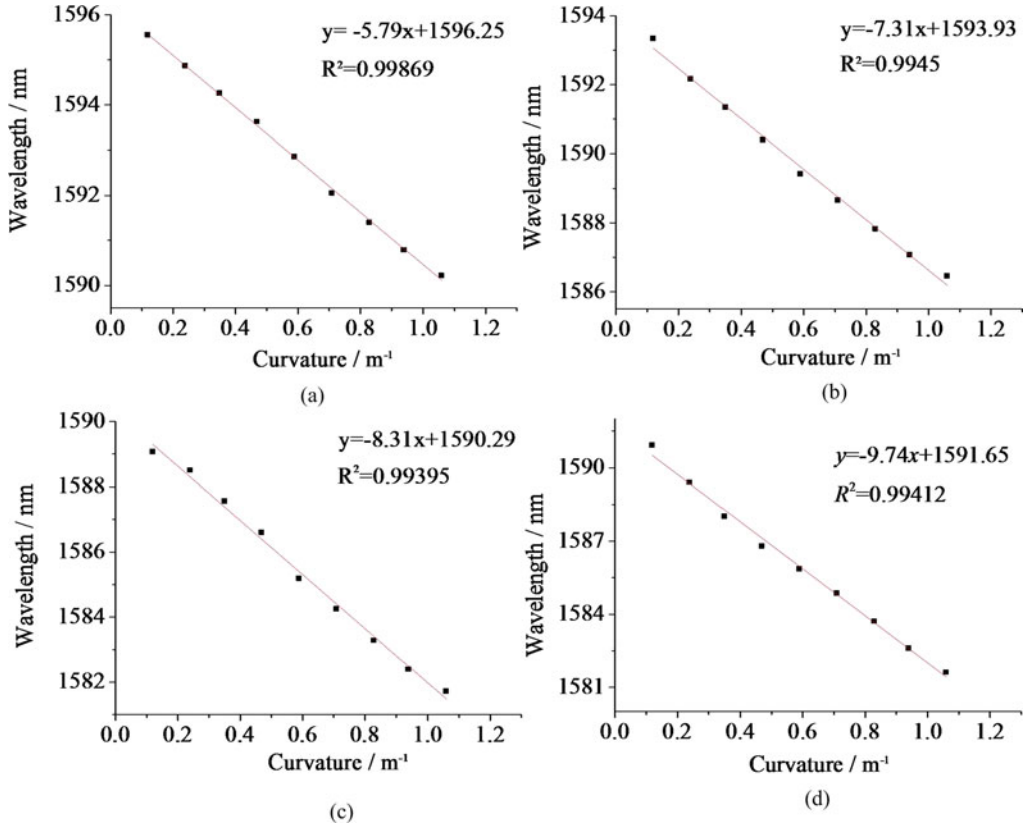

Fig. 11. Relationship between wavelength shift and curvature for convex bending with different sensor length. (a) 10 mm. (b) 13 mm. (c) 16 mm. (d) 19 mm.

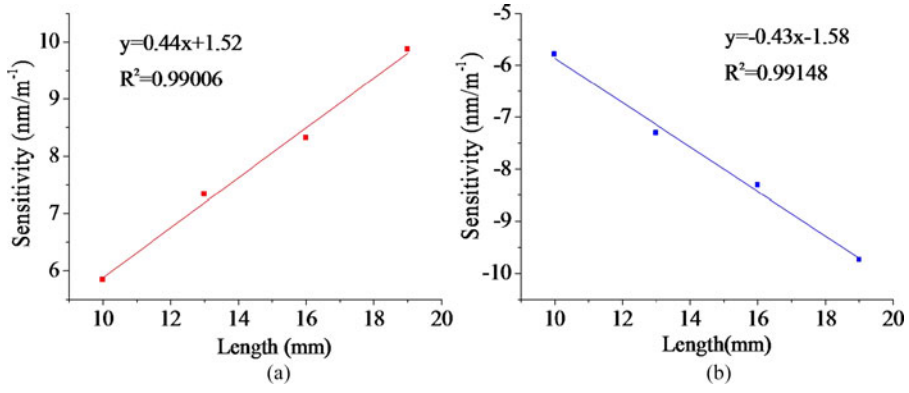

Fig. 12. Relationship between sensor length and curvature sensitivity. (a) Concave bending. (b) Convex bending.

respectively, the corresponding curvature sensitivity are -5.79 nm/m^{-1}, -7.31 nm/m^{-1}, -8.31 nm/m^{-1}, and -9.74 nm/m^{-1} separately. The curvature sensitivity of the four groups of sensors for concave and convex bending is summarized, and the relationship between the sensor length and the curvature sensitivity is obtained by the scanning point method, as shown in Fig. 12.

It can be learned from Fig. 12, for sensors with different lengths in concave bending and convex bending, phenomena of red shift and blue shift will take place respectively. And with the increase of the sensor length, the phenomena of red and blue shift in concave and convex bending are more and more obvious. Each 1 mm increasing of the sensor length would separately cause an

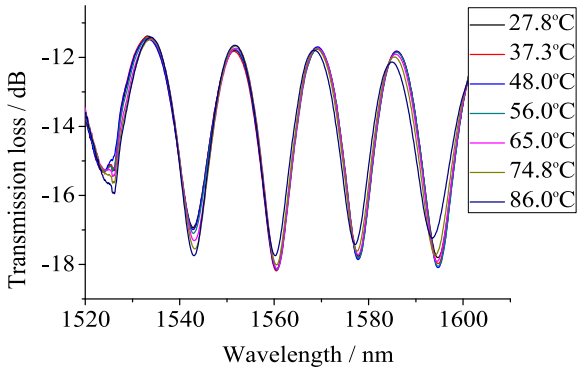

Fig. 13. Transmission spectrum at different temperatures.

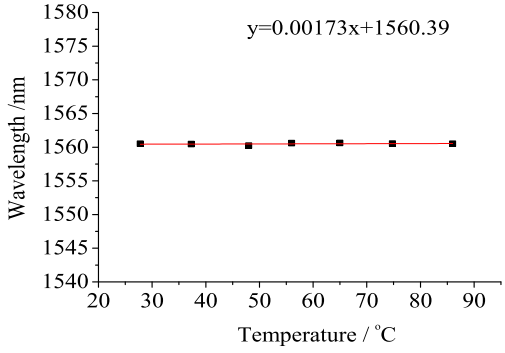

Fig. 14. Relationship between wavelength shift and temperature.

average increase in the corresponding sensitivity of 0.44 nm/m^{-1} and -0.43 nm/m^{-1} for concave and convex bending. The results show that the curvature sensitivity is, indeed, with the increase of the sensor length, and it is known from (5) that the longer L is, the greater the shift amount of the corresponding interference fringes of the sensor are, then the higher the sensitivity of the sensor is. The experimental results coincide with the theoretical analysis very well.

3.4 Temperature Sensing Experiment

In the temperature sensing experiment, place and fix the sensor with length of 16 mm on the glass sheet, then put it in the temperature control experiment box. Connect SMF at the two ends of the sensor to the ASE light source and OSA respectively.

Through setting different temperature value on the temperature control box, the measurement of different temperature can be performed. Set the temperature changes in the range of 20∼90 °C on the control box. Stabilize for 20 minutes and record the spectrum after the temperature reaches the preset value each time. The temperature is measured every 10 °C. The corresponding transmission spectra at different temperatures are shown in Fig. 13.

It is visible from Fig. 13, with the increase of temperature, the transmission spectrum of the sensor has a slight shift to the long wave direction. Analyze the transmission spectrum, and calculate the wavelength shift in the vicinity of 1560 nm trough, thus the relationship between wavelength shift and temperature can be gained, as shown in Fig. 14. At this point, the temperature sensitivity of the sensor is only 1.73 pm/°C, which indicates it is insensitive to temperature.

The main reason for its insensitivity to temperature lies in when the ambient temperature changes, due to the influence of thermo-optic effect and thermal expansion effect, the refractive index of the fiber is changed, causing the wavelength shift of the sensor transmission spectrum. The shift of the center wavelength [17] on *m* order interference fringe caused by ambient temperature change can

be regarded as

$$\Delta\lambda_m^1 = (\alpha + p_t)\,\lambda_m \Delta T \tag{11}$$

where p_t represents change of effective refractive index difference between the two modes produced interference when the external temperature is changed, α is the material's thermal expansion coefficient, ΔT is the external temperature change. Because PCF is mainly composed of SiO_2, and its thermal expansion coefficient is only 5×10^{-7} /°C, the material thermal expansion effect caused by the temperature difference is very small, which leads to its little impact on the change of transmission mode. For this reason, the variation of p_t caused by it is approximate to zero. As a consequence, the sensor prepared by PCF in this article is insensitive to temperature, which avoids the cross-sensitivity of temperature and curvature when measured together.

Thereby, the PCF curvature sensor with core-offset splicing and waist-enlarged fiber taper character is not only easy to be produced but also has the ability to identify the direction, and has higher curvature sensitivity. According to the experimental results of the curvature and temperature, it shows that when the sensor is in convex and concave bending, as the curvature increasing, interference spectrum respectively occurs to blue and red shift, and there is a good linear relationship between wavelength shift and the change of curvature. As the result, PCF curvature sensor characterized by core-offset splicing and waist-enlarged fiber taper can measure the direction and the size of the curvature simultaneously. In addition, PCF curvature sensor has the characteristics of temperature insensitive, and can effectively avoid the cross-sensitivity problem of the temperature and the curvature in the measurement process.

In 20∼90 °C, the total wavelength shift is only 0.39 μm for this sensor. Especially, these experiments are carried out at room temperature, and lead to a smaller temperature changing. Moreover, the temperature sensitivity of the sensor is only 1.73 pm/°C. That is, the wavelength shift is only 1.73 pm for each degree change in temperature. This shift is minor compared to the wavelength shift in curvature measurements. Thereby, we can strip the influence of temperature when doing curvature sensing.

4. Conclusion

In this paper a PCF curvature sensor characterized by core-offset splicing and waist-enlarged fiber taper is described in detail. It is produced by separately connecting the two ends of PCF to SMF by core-offset splicing and excessive splicing method. The experimental results show that for sensors with length of 10 mm, 13 mm, 16 mm, and 19 mm and in the curvature range of 0.12∼1.06 m^{-1}, the curvature sensitivity for concave bending are 5.84 nm/m^{-1}, 7.33 nm/m^{-1}, 8.32 nm/m^{-1}, and 9.87 nm/m^{-1} and, for convex bending, are 5.79 nm/m^{-1}, 7.31 nm/m^{-1}, 8.31 nm/m^{-1}, and 9.74 nm/m^{-1}, respectively. Sensors with different lengths for concave bending and convex bending occur to red and blue shift seperatedly, and with the increase of sensor length, the shift phenomena are more and more obvious. Each 1 mm length increase can lead to the sensitivity of its corresponding bending average increased by 0.44 nm/m^{-1} and 0.43 nm/m^{-1}. The longer the sensor length is, the greater the interference fringe shift of the corresponding sensor is, and the higher the curvature sensitivity of the sensor is. They have good linearity. For sensor with length of 16 mm, its temperature sensitivity is only 1.73 pm/°C, insensitive to temperature. Compared with other types of curvature sensor, the sensor proposed in this article has the advantages of easy preparation, high sensitivity, and the ability of direction recognition. The sensor is insensitive to temperature, which avoid the problem of cross-sensitivity of temperature and curvature measured meantime. It definitely has a good application prospect in the fields of aerospace, large machinery, and so on.

References

[1] J. Su *et al.*, "High sensitivity multimode-multimode-multimode structure fiber sensor based on modal interference," *Opt. Commun.*, vol. 315, pp. 112–115, Mar. 2014.

[2] C. Zhang *et al.*, "High-sensitivity all single-mode fiber curvature sensor based on bulge-taper structures modal interferometer," *Opt. Commun.*, vol. 336, no. 20, pp. 197–201, Feb. 2015.
[3] J. Chen *et al.*, "Optical fiber curvature sensor based on few mode fiber," *Optik*, vol. 125, no. 17, pp. 4776–4778, Sep. 2014.
[4] T. K Yadav *et al.*, "Single mode tapered fiber-optic interferometer based refractive index sensor and its application to protein sensing," *Opt. Exp.*, vol. 22, no. 19, pp. 22802–22807, Sep. 2014.
[5] Z. Li *et al.*, "Temperature-insensitive refractive index sensor based on in-fiber Michelson interferometer," *Sensors Actuators B, Chem.*, vol. 199, no. 4, pp. 31–35, Aug. 2014.
[6] W. Cui *et al.*, "Compact bending sensor based on a fiber bragg grating in an abrupt biconical taper," *Opt. Exp.*, vol. 23, no. 9, pp. 11031–11036, May 2015.
[7] G. Jorge *et al.*, "Temperature-independent curvature sensor using FBG cladding modes based on a core misaligned splice fiber," *IEEE Photon. Technol. Lett.*, vol. 23, no. 12, pp. 804–806, Jun. 2011.
[8] D. Wu *et al.*, "In-line fiber Fabry-Perot refractive index tip sensor based on photonic crystal fiber and spectrum differential integration method," *Opt. Commun.*, vol. 313, no. 44, pp. 270–275, Feb. 2014.
[9] M. Jiang *et al.*, "Temperature-independent optical fiber Fabry–Perot refractive-index sensor based on hollow-core photonic crystal fiber," *Optik*, vol. 125, no. 13, pp. 3295–3298, Jul. 2014.
[10] Y. Zheng *et al.*, "Optical fiber magnetic field sensor based on magnetic fluid and microfiber mode interferometer," *Opt. Commun.*, vol. 336, pp. 5–8, Feb. 2014.
[11] P. Geng *et al.*, "Two-dimensional bending vector sensing based on spatial cascaded orthogonal long period fiber," *Opt. Exp.*, vol. 20, no. 27, pp. 28557–28562, Dec. 2012.
[12] B. Dong, J. Hao, and Z. Xue, "Temperature insensitive curvature measurement with a core-offset polarization maintaining photonic crystal fiber based interferometer," *Opt. Fiber Technol.*, vol. 17, pp. 233–235, Jan. 2011.
[13] S. Li *et al.*, "Bending sensor based on intermodal interference properties of two-dimensional waveguide array fiber," *Opt. Lett.*, vol. 37, no. 10, pp. 1610–1612, May 2012.
[14] X. Wen *et al.*, "Ultrasensitive temperature fiber sensor based on Fabry-Pérot interferometer assisted with iron Vgroove," *Opt. Exp.*, vol. 23, no. 9, pp. 11526–11536, May 2015.
[15] L. Mao *et al.*, "Highly sensitive curvature sensor based on single-mode fiber using core-offset splicing," *Opt. Laser Technol.*, vol. 57, pp. 39–43, Apr. 2014.
[16] H. Gong *et al.*, "Curvature sensor based on hollow-core photonic crystal fiber sagnac interferometer," *IEEE Sensors J.*, vol. 14, no. 3, pp. 777–780, Mar. 2014.
[17] H. Sun *et al.*, "High sensitivity optical fiber temperature sensor based on the temperature cross-sensitivity feature of RI-sensitive device," *Opt. Commun.*, vol. 313, no. 14, pp. 28–31, Jul. 2014.